Zero3D: Semantic-Driven 3D Shape Generation For Zero-shot Learning

Bo Han · Yitong Fu · Yixuan Shen

Abstract Semantic-driven 3D shape generation aims to generate 3D shapes conditioned on textual input. However, previous approaches have faced challenges with the single-category generation, low-frequency details, and the requirement for large quantities of paired data. To address these issues, we propose a multi-category diffusion model. Specifically, our approach includes the following components: 1) To mitigate the problem of limited large-scale paired data, we establish a connection between text, 2D images, and 3D shapes through the use of the pre-trained CLIP model, enabling zeroshot learning. 2) To obtain the multi-category 3D shape feature, we employ a conditional flow model to generate a multi-category shape vector conditioned on the CLIP embedding. 3) To generate multi-category 3D shapes, we utilize a hidden-layer diffusion model conditioned on the multi-category shape vector, resulting in significant reductions in training time and memory consumption. We evaluate the generated results of our framework and demonstrate that our method outperforms existing methods.

Keywords 3D Shape Generation · Point-Cloud · Diffusion Model

1 Introduction

As a core element in the Metaverse world [26], 3D objects play a vital role in enhancing user interactivity.

Bo Han

Zhejiang University E-mail: borishan815@zju.edu.cn

Yitong Fu

Zhejiang University E-mail: yitong@zju.edu.cn

Yixuan Shen

National University Singapore E-mail: Matilda_shenyixuan@outlook.com

With the rapid development of AIGC technology [6, 10], it has become increasingly easy to create images, audio, and video through text prompts. However, the design of 3D objects still relies on manual modeling software such as Blender and Maya3D, which requires significant time and expertise. As such, the generation of high-quality 3D objects through semantic information has become a practical challenge.

Unlike 2D images, which can be represented as arrays of pixel values, 3D objects have diverse and complex representations, including voxels [31], point clouds [16], grids [13], and implicit representations [2]. Each representation has its own advantages and limitations, and different representations require different processing methods, adding to the challenge [24].

Text to 3D shape generation is also challenging [8, 25] due to the difficulty of jointly understanding 3D shapes and text and representing them in a common space. Furthermore, unlike text to image generation where paired data is abundant, text to 3D shape generation lacks large-scale paired text and 3D shape data.

Recent work on 3D shape generation [12, 15, 16, 19] has yielded promising results. DreamFusion [19], for example, transforms the diffusion and denoising processes in pixel space into operations in the NeRF parameter space [17]. However, due to the use of low-resolution images (64 x 64) as supervision signals, DreamFusion [19] is unable to synthesize high-frequency 3D geometric and texture details. DPM [16] trains an encoder to generate a shape vector representing a point cloud shape, which is then used to train a flow model. The pretrained flow model can then convert noise into a shape vector, and the diffusion model utilizes this shape vector as a condition for 3D shape generation. However, since DPM [16] is trained on a specific category, it can only generate point cloud data of one type.

To address these challenges, we first pre-train a CLIP model [6] to establish a superior correspondence between text and 2D images. We can also obtain a large number of high-resolution 2D images corresponding to 3D objects through the use of Blender. As such, the CLIP model bridges text, 2D images, and 3D objects, mitigating the problem of limited large-scale paired text-3D shape data. We then apply a conditional flow model [5] to generate a multi-category shape vector conditioned on the CLIP embedding. Subsequently, we employ a conditional diffusion model to generate the 3D point cloud data conditioned on the multi-category shape vector. Specifically, during training, the CLIP model is used to encode the 2D image as a condition, allowing the model to learn the correspondence between the 2D image and the 3D point cloud. During inference, the CLIP model encodes semantic information as a condition, enabling the generation of 3D point cloud corresponding to the semantic information. Additionally, to address the high time and memory consumption of the diffusion model itself, we implement the diffusion process and denoising operation on the hidden layer.

To summarize, our main contributions are:

- Considering the superior correspondence between 2D images and texts in the CLIP model, We establish a connection between texts and 3D shapes by using 2D images as a medium, thereby enabling zero-shot learning.
- We propose a multi-category diffusion framework capable of generating 3D point cloud data for multiple categories using a single network model.

2 Background

2.1 3D Shape Generation

Some widely used generative models currently include the Variational Autoencoder (VAE) [14], Generative Adversarial Network (GAN) [7], Flow model [21], and Diffusion model [9]. 3D-GAN [28] first employs a 3D-CNN to gradually map a high-dimensional hidden vector into a 3D object represented by voxels. r-GAN [27] utilizes Graph Convolutional Network as the generator, effectively leveraging local information within point cloud data. However, due to the inherent uncertainty of Generative Adversarial Networks [4], the results are not always ideal. PointFlow [29] introduces a flow model to generate the shape distribution of point clouds, using a hidden vector representing the shape distribution as a condition to guide point cloud generation. However, since point clouds are typically distributed on a two-dimensional manifold, it is difficult to obtain better results using a flow model that assumes the point

cloud follows a three-dimensional prior distribution. In the 3D domain, DPM [16] and PVD [31] use diffusion models to generate point cloud data. Although they can produce satisfactory results, they are both trained on specific categories.

2.2 Semantic-Driven 3D Shape Generation

Text2Shape [1] proposes an end-to-end association learning framework that separately encodes text and 3D shapes into the same latent space. However, large-scale text-3D shape data is still difficult to obtain, so Clip-Forge [22] bypasses this problem with the aid of the CLIP model for text-image matching. CLIP-Mesh [18] employs the CLIP model to assess the degree of correspondence between images and text, enabling direct optimization of mesh model parameters. Similarly, Avatar-CLIP [11] utilizes the CLIP model to facilitate semantically driven generation of 3D human body models. This is achieved by optimizing SMPL model parameters through the learning of correspondences between differentiably rendered images and input text. Dreamfields [12], DreamFusion [19], and Magic3D [15] all use NeRF [17] as an implicit representation of 3D objects and render images through differentiable renderers. They utilize the degree of match between images and text to optimize the entire network and ultimately extract the 3D mesh model from the optimized implicit neural field representation.

3 Method

The schematic overview of our proposed architecture is illustrated in Fig. 1. The left side of the figure shows the training architecture, which consists of four main components: a shape encoder, a CLIP model, a conditional flow model, and a conditional diffusion model. We use the DPM model as our backbone, which samples noise data from a Gaussian distribution and generates point cloud data through a denoising process under the given condition. Specifically, during training, we divide our model into two tasks. First, we render 3D objects to obtain high-resolution 2D images, which are then used as input to the pre-trained CLIP model. We use the shape encoder to obtain the shape parameter vector of multi-category 3D point cloud data, and then the conditional flow model is trained to establish the relationship between the CLIP embedding and the multi-category shape vector. Next, we use the multicategory shape vector as a condition to guide 3D shape generation in the diffusion model. During inference, the text is used as input to the CLIP model. Based on the

bi-directionality of the flow model, we can obtain the shape vector guided by the CLIP embedding. Subsequently, the shape vector guides the diffusion model to generate multi-category point clouds. In this way, we use readily available 2D images as a medium to establish the connection between 3D point cloud data and text data, enabling zero-shot learning.

3.1 Shape Encoder

The model maps point cloud data to a distribution of shape vectors, namely the shape mean and shape variance, and then samples a shape vector from the shape mean and variance. The overall network comprises a feature extraction layer and a distribution mapping layer. For the feature extraction layer, we use a series of 1D convolutional layers to increase the dimensionality of the point cloud data, followed by selecting the maximum value of each dimension feature to perform feature dimension reduction. For the distribution mapping layer, the data after feature dimension reduction is mapped to the shape mean and variance, respectively, to represent the distribution of the point cloud shape vector. Subsequently, an offset value ε is randomly generated to sample a shape vector s, as defined in Equation 1.

$$s = \mu + \epsilon * \exp(0.5 * \log(\sigma^2))$$
 (1)

3.2 CLIP Model

The CLIP model encodes text and 2D images into the same latent space, enabling the matching of images and text. Based on the CLIP model, we learn the correspondence between 3D point clouds and text using images as an intermediary. The CLIP model is based on the VisualTransformer [6] and uses the ViT-B/32 model to match images to 16x16 text vectors. During the training and inference stage, images or text are passed through the CLIP model to obtain a one-dimensional vector of length 256, which is normalized and input into the conditional flow model as a condition.

3.3 Conditional Flow Model

Unlike traditional VAE models [14], which encode data into a standard normal distribution, the flow model can learn a more flexible and variable distribution. The shape vector is fed into the conditional flow model to learn the transformation from the Gaussian noise distribution to the distribution of multi-category shape

features, with the CLIP embedding serving as the condition. During inference, data is directly sampled from the Gaussian distribution, and the corresponding shape vector is obtained through the inverse transformation of the flow model. This shape vector is then input into the diffusion model as a condition. We use the affine transformation layer in the RealNVP network architecture [5] to construct the flow model. The affine transformation layer divides the input into two parts: the first part remains unchanged, while the second part is transformed using scale and offset coefficients. For an input x that is D-dimensional, the forward calculation for the output y of the affine coupling layer is as follows:

$$y_{1:d} = x_{1:d}$$

$$y_{d+1:D} = x_{d+1:D} \odot \exp(s(x_{1:d})) + t(x_{1:d})$$
(2)

The inverse calculation for the output x is as follows:

$$x_{1:d} = y_{1:d} x_{d+1:D} = (y_{d+1:D} - t(y_{1:d})) \odot \exp(-s(y_{1:d}))$$
(3)

Since the first part of the input is directly the output, if each layer is divided into two parts in the same way, the first part of the input and output of the entire flow model will remain unchanged. To enhance the model's ability to process data and produce a more balanced output, we adopt an alternating mask approach. In this approach, odd-numbered layers use the first d-dimensional data as the first part and the last D-d dimensional data as the second part, while even-numbered layers do the opposite.

3.4 Point Cloud Autoencoder

To reduce the computational time and memory consumption of the diffusion model, we first train a point cloud autoencoder, with the encoded hidden vector serving as input to the subsequent diffusion model for 3D shape generation. The output of the denoising process diffusion model is decoded into point cloud data by the point cloud decoder. The point cloud autoencoder comprises an encoder and a decoder. The encoder is primarily based on the PointNet network architecture [20] and the graph-based max pooling layer [23], while the decoder is primarily based on FoldingNet [30]. Fig. 2 shows the network architecture of the point cloud autoencoder.

The goal of the point cloud autoencoder is to restore the original point cloud shape as accurately as possible. To achieve this, we use the point cloud reconstruction loss, calculated using the Chamfer Distance.

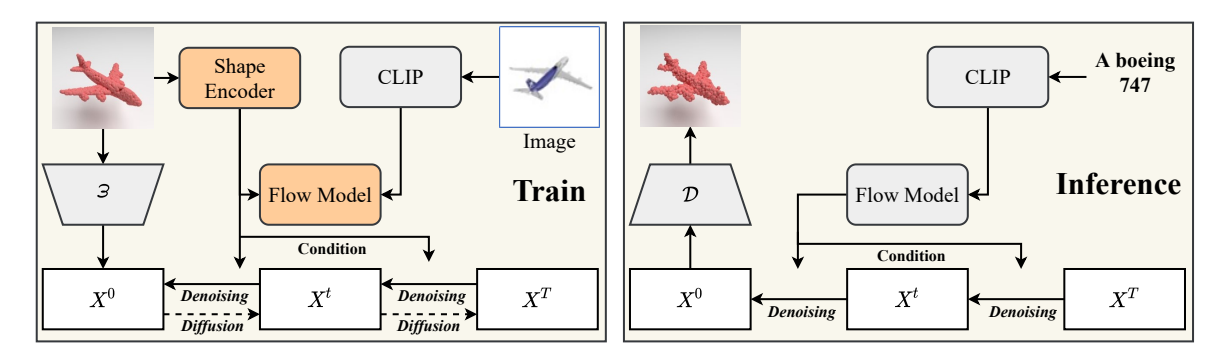


Fig. 1 The left image represents the training stage, while the right image represents the inference stage. The gray modules ε and \mathcal{D} , representing the encoder and decoder in the point cloud autoencoder, respectively, are pre-trained in advance. The CLIP model uses the Visual Transformer [6] ViT-B/32 checkpoint. During the training phase, the conditional flow model and point cloud diffusion model are jointly trained on 2D image and 3D point cloud data. During the inference stage, text data is used to drive and generate corresponding 3D point cloud data.

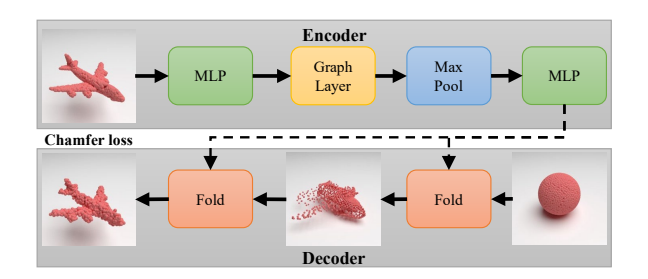


Fig. 2 Point Cloud Autoencoder network architecture

The Chamfer Distance between two point sets S_1 and S_2 in 3D point cloud reconstruction is calculated by finding the closest point in S_2 for each point in S_1 and then calculating the L2 distance. The average of the distances calculated for each point in S_1 is then taken, as shown in the following Equation 4:

$$Ch(S_1, S_2) = \sum_{p_1 \in S_1} \min_{p_2 \in S_2} \|p_1 - p_2\|_2$$
(4)

For two point sets, the mutual Chamfer Distance must be calculated, resulting in the final distance formula shown in Equation 5. In this formula, N_{S_1} and N_{S_1} represent the number of points in the two point sets, respectively.

$$d_{ch}(S_{1}, S_{2}) = \frac{1}{N_{S_{1}}} Ch(S_{1}, S_{2}) + \frac{1}{N_{S_{2}}} Ch(S_{2}, S_{1})$$

$$= \frac{1}{N_{S_{1}}} \sum_{p_{1} \in S_{1}} \min_{p_{2} \in S_{2}} \|p_{1} - p_{2}\|_{2}$$

$$+ \frac{1}{N_{S_{2}}} \sum_{p_{2} \in S_{2}} \min_{p_{1} \in S_{1}} \|p_{2} - p_{1}\|_{2}$$
(5)

3.5 Conditional Diffusion Model

The diffusion model consists of a diffusion process and a denoising process. The diffusion process gradually adds noise to the point cloud hidden vector, converting a point cloud distribution of a specific shape into a random noise Gaussian distribution. The denoising process transforms noisy data into the point cloud hidden vector, with the shape vector s serving as the condition. Based on the diffusion model, point cloud data can be considered as a set of points randomly sampled from a specific distribution. These points follow the same distribution but are independent of each other, meaning that point cloud data can be expressed as $\mathbf{X}^{(0)} = \left\{x_i^{(0)}\right\}_{i=1}^N.$ We train the diffusion model using the hidden layer vector, so in this case, $\mathbf{X}^{(0)}$ represents the hidden layer vector encoded by the point cloud encoder. The diffusion process can be expressed as follows:

$$q\left(x_{i}^{(t)} \mid x_{i}^{(t-1)}\right) = \mathcal{N}\left(x_{i}^{(t)} \mid \sqrt{1 - \beta_{t}} x_{i}^{(t-1)}, \beta_{t} \mathbf{I}\right)$$
(6)

$$q\left(x_{i}^{1:T} \mid x_{i}^{(0)}\right) = \prod_{t=1}^{T} q\left(x_{i}^{(t)} \mid x_{i}^{(t-1)}\right) \tag{7}$$

where $\beta_1...\beta_T$ are hyperparameters at each time step that controls the noise addition process.

The denoising process aims to recover the original point cloud hidden vector from the noise data. First, the point cloud hidden vector is sampled from the noise distribution, and then, through a reverse Markov chain, the noise is gradually subtracted. Under the condition of the shape vector s, the denoised diffusion process can be expressed as follows:

$$p_{\theta}\left(x^{(t-1)} \mid x^{(t)}, s\right) = \mathcal{N}\left(x^{(t-1)} \mid \mu_{\theta}\left(x^{(t)}, t, s\right), \beta_{t}\mathbf{I}\right)$$
(8)

$$p_{\theta}\left(x^{(0:T)} \mid s\right) = p\left(x^{(T)}\right) \prod_{t=1}^{T} p_{\theta}\left(x^{(t-1)} \mid x^{(t)}, s\right)$$
 (9)

Among them, μ_{θ} is a mean value estimated by the neural network, s is the conditional shape vector, and the initial data of inverse diffusion obeys the standard normal distribution N(0, I).

Since the overall point cloud data can be considered as a collection of sampling points that follow the same distribution, the probability of the overall point cloud data can be expressed by the probability of each individual point:

$$q\left(\mathbf{X}^{(1:T)} \mid \mathbf{X}^{0}\right) = \prod_{i=1}^{N} q\left(x_{i}^{(1:T)} \mid x_{i}^{(0)}\right)$$

$$p_{\theta}\left(\mathbf{X}^{(0:T)} \mid s\right) = \prod_{i=1}^{N} p_{\theta}\left(x_{i}^{(0:T)} \mid s\right)$$

$$(10)$$

The training objective is to maximize the likelihood function of the generated point cloud data $E\left[\log p_{\theta}\left(\mathbf{X}^{(0)}\right)\right]$. Similar to the VAE model, the specific optimization goal is still to maximize its variational lower bound.

$$\mathbb{E}[\log p_{\theta}(\mathbf{X}^{(0)})] \geq \mathbb{E}\left[\log \frac{p_{\theta}(\mathbf{X}^{(0:T)}, s)}{q(\mathbf{X}^{(1:T)}, s|\mathbf{X}^{(0)})}\right]$$

$$= \mathbb{E}\left[\log p(\mathbf{X}^{T})\right]$$

$$+ \sum_{t=1}^{T} \log \frac{p_{\theta}(\mathbf{X}^{(t-1)}|\mathbf{X}^{(t)}, s)}{q(\mathbf{X}^{(t)}|\mathbf{X}^{(t-1)})}$$

$$- \log \frac{q_{\phi}(s|\mathbf{X}^{(0)})}{p(s|c)}$$
(11)

In the above equation, c represents the condition of the flow model, i.e., the embedding encoded by the CLIP model, while s represents the condition of the diffusion model, i.e., the shape vector. In the last step of the inverse diffusion process, the resulting data, denoted as $\mathbf{X}^{(0)}$, is known and thus treated separately. The optimization objective can be formulated to minimize the loss function L:

$$L(\theta, \phi) = \mathbb{E}_{q} \left[\sum_{t=2}^{T} D_{KL} \left(\underbrace{q \left(\mathbf{X}^{(t-1)} \mid \mathbf{X}^{(t)}, \mathbf{X}^{(0)} \right)}_{(1)} \right) \right]$$

$$\underbrace{p_{\theta} \left(\mathbf{X}^{(t-1)} \mid \mathbf{X}^{(t)}, s \right)}_{(2)} \cdot -\log p_{\theta} \left(\mathbf{X}^{(0)} \mid \mathbf{X}^{(1)}, s \right) \right]$$

$$+D_{KL} \left(\underbrace{q_{\phi} \left(s \mid \mathbf{X}^{(0)} \right)}_{(4)} \right) \underbrace{p(s \mid c)}_{(5)}$$

$$(12)$$

In Equation 12, $q(\mathbf{X}^{(t-1)} \mid \mathbf{X}^{(t)}, \mathbf{X}^{(0)})$ is a known Gaussian distribution, which can be calculated by the following equation:

$$q\left(\mathbf{X}^{(t-1)} \mid \mathbf{X}^{(t)}, \mathbf{X}^{(0)}\right) = \mathcal{N}\left(x_i^{(t-1)} \mid \mu_t\left(x^{(t)}, x^{(0)}\right), \gamma_t \mathbf{I}\right)$$
(13)

After substituting variables for $\alpha_t = 1 - \beta_t$, $\bar{\alpha}_t = \prod_{s=1}^t \alpha_s$, the mean and variance in the Equation 13 can be expressed as:

$$\mu_{t}\left(x^{(t)}, x^{(0)}\right) = \frac{\sqrt{\bar{\alpha}_{t-1}}\beta_{t}}{1 - \bar{\alpha}_{t}}x^{(0)} + \frac{\sqrt{\alpha_{t}}\left(1 - \bar{\alpha}_{t-1}\right)}{1 - \bar{\alpha}_{t}}x^{(t)}$$

$$\gamma_{t} = \frac{1 - \bar{\alpha}_{t-1}}{1 - \bar{\alpha}_{t}}\beta_{t}$$
(14)

 $p_{\theta}\left(\mathbf{X}^{(t-1)} \mid \mathbf{X}^{(t)}, s\right)$ and $p_{\theta}\left(\mathbf{X}^{(0)} \mid \mathbf{X}^{(1)}, s\right)$ are Gaussian distributions obtained by neural network training. Through reparameterization, the output data and the noise data ε can be used as \mathcal{L}_2 loss to optimize the network:

$$L(\theta) = \left\| \epsilon - \epsilon_{\theta} \left(x_i^{(t)}, t, s \right) \right\|^2, \epsilon \sim \mathcal{N}(0, \mathbf{I})$$
 (15)

where t is sampled uniformly between 1 and T, and ϵ_{θ} is the learned diffusion model.

4 Experiments

4.1 Dataset

We use the ShapeNet V2 processed dataset [3], which contains 13 categories of data, with each sample comprising point cloud data and corresponding 2D rendered images of each 3D object. To ensure a fair comparison, we adopt the same dataset-splitting approach.

	Airplane		chair		Car	
Method	CD	EMD	CD	EMD	CD	EMD
r-GAN [27]	97.3	95.2	86.2	89.6	91.7	98.7
PointFlow [29]	78.2	78.1	67.2	67.2	58.1	54.7
PVD [31]	76.8	67.8	60.5	56.9	59.0	54.5
Ours-P	80.1	71.2	64.8	58.2	65.3	61.7
Ours	77.3	65.7	61.8	54.4	57.1	54.0

Table 1 CD and EMD metrics results on three categories

4.2 Evaluation Metrics

For single-class generation, we use the Chamfer Distance and Earth Mover's Distance to evaluate the reconstruction quality following prior works [27, 29, 31].

Chamfer Distance (CD) It calculates the average minimum distance between each generated point and its closest point in the ground-truth point cloud.

Earth Mover's Distance (EMD) It measures the dissimilarity between two distributions, taking into account both their shape and relative position.

For semantic-driven generation, Zero3D enables zeroshot training, eliminating the need for 3D data with associated compound text labels. While this offers significant advantages in terms of training and application scalability, it also results in the absence of real data corresponding to the text during evaluation. In line with previous research, we assess composite textdriven point cloud data using the CLIP R-precision employed in DreamFields [12].

CLIP R-precision It evaluates the generation effect with composite text by ranking results between textual descriptions and generated images. The higher the ranking of the real text, the higher the quality of the generated data.

	CLIP R-precision ↑			
Method	CLIP B/32	CLIP B/16	CLIP $L/14$	
DreamFusion [19]	42.5	44.6	58.5	
Ours-P	31.5	35.1	40.8	
Ours	32.8	34.1	41.5	

Table 2 CLIP R-precision comparison results

4.3 Results

The point cloud data generated using the single-category word is shown in Fig. 4 and Table 1. Evaluation results demonstrate Zero3D is competitive with the state-of-the-art methods for text-to-point cloud generation in terms of CD and EMD metrics and often outperforms in terms of EMD. Additionally, compared to other text

to point cloud methods, Zero3D can support the generation of multiple categories with a single model and exhibits superior integration and scalability. This is due to Zero3D's ability to better capture the shape vector of point cloud. The point cloud data generated using composite text is shown in Fig. 3 and Table 2. As there are no open-source works on composite text-to-point cloud generation for comparison, we can only compare our results to DreamFusion [19]. Although DreamFusion [19] employs a different method and generates 3D data representations using Nerf rather than point clouds, it can still be inferred from Table 2 that Zero3D is capable of generating believable 3D point clouds using semantic information.

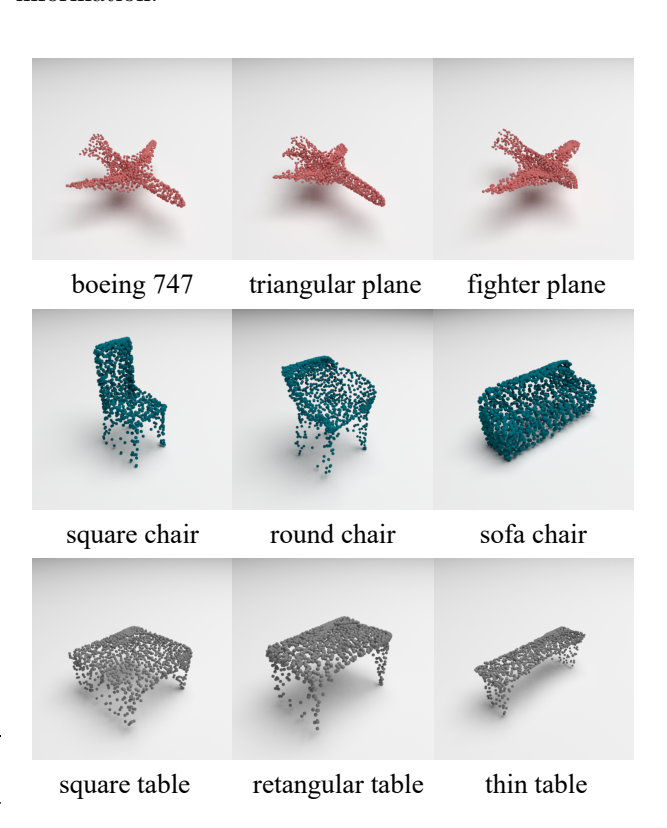


Fig. 3 Point cloud generated from composite text

4.4 Ablation Study

To validate the efficacy of our approach in enhancing results through the implementation of a point cloud diffusion model on the hidden layer, we conducted ablation experiments. The diffusion model based on the original point cloud, denoted as Our-P, involves directly inputting 3D point cloud data into the diffusion model for training without passing through the point cloud autoencoder. As demonstrated in Tables 1 and 2, the point

cloud diffusion model based on the hidden layer outperforms the diffusion model based on the original point cloud in both single-category and composite text-driven point cloud generation tasks. Furthermore, as shown in Table 3, the point cloud diffusion model based on the hidden layer exhibits superior performance in terms of memory usage and time consumption compared to the diffusion model based on the original point cloud.

Method	Convergence epoch	epoch time	Memory
ours-P	280000	$\begin{array}{c} 0.09 \mathrm{s} \\ 0.03 \mathrm{s} \end{array}$	11057MB
ours	220000		8102MB

Table 3 Memory usage and time consumption comparision

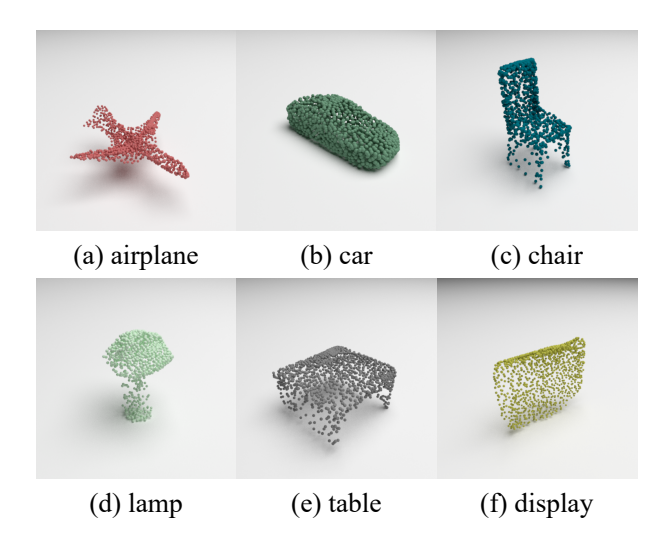


Fig. 4 Point cloud generated from the corresponding word

5 Conclusion

In this paper, we propose a zero-shot learning framework that establishes the relationship between 3D point clouds and text through the intermediary of 2D images. This approach can generate multi-category point clouds and alleviate the gap caused by the lack of large-scale text-3D point cloud data pairs. By implementing the diffusion and denoising processes on the hidden layer, training speed and memory usage are greatly optimized.

References

1. Chen, K., Choy, C.B., Savva, M., Chang, A.X., Funkhouser, T., Savarese, S.: Text2shape: Generating shapes from natural language by learning

- joint embeddings. arXiv preprint arXiv:1803.08495 (2018)
- Chiang, P.Z., Tsai, M.S., Tseng, H.Y., Lai, W.S., Chiu, W.C.: Stylizing 3d scene via implicit representation and hypernetwork. In: Proceedings of the IEEE/CVF Winter Conference on Applications of Computer Vision, pp. 1475–1484 (2022)
- 3. Choy, C.B., Xu, D., Gwak, J., Chen, K., Savarese, S.: 3d-r2n2: A unified approach for single and multiview 3d object reconstruction. In: ECCV, pp. 628–644. Springer (2016)
- Creswell, A., White, T., Dumoulin, V., Arulkumaran, K., Sengupta, B., Bharath, A.A.: Generative adversarial networks: An overview. IEEE signal processing magazine 35(1), 53–65 (2018)
- 5. Dinh, L., Sohl-Dickstein, J., Bengio, S.: Density estimation using real nvp. arXiv preprint arXiv:1605.08803 (2016)
- Dosovitskiy, A., Beyer, L., Kolesnikov, A., Weissenborn, D., Zhai, X., Unterthiner, T., Dehghani, M., Minderer, M., Heigold, G., Gelly, S., et al.: An image is worth 16x16 words: Transformers for image recognition at scale. In: ICLR (2020)
- Goodfellow, I., Pouget-Abadie, J., Mirza, M., Xu, B., Warde-Farley, D., Ozair, S., Courville, A., Bengio, Y.: Generative adversarial networks. Communications of the ACM 63(11), 139–144 (2020)
- Han, Z., Shang, M., Wang, X., Liu, Y.S., Zwicker, M.: Y2seq2seq: Cross-modal representation learning for 3d shape and text by joint reconstruction and prediction of view and word sequences. In: AAAI, vol. 33, pp. 126–133 (2019)
- 9. Ho, J., Jain, A., Abbeel, P.: Denoising diffusion probabilistic models. Advances in Neural Information Processing Systems **33**, 6840–6851 (2020)
- Ho, J., Salimans, T., Gritsenko, A., Chan, W., Norouzi, M., Fleet, D.J.: Video diffusion models. arXiv preprint arXiv:2204.03458 (2022)
- Hong, F., Zhang, M., Pan, L., Cai, Z., Yang, L., Liu, Z.: Avatarclip: Zero-shot text-driven generation and animation of 3d avatars. ACM Transactions on Graphics (TOG) 41(4), 1–19 (2022)
- Jain, A., Mildenhall, B., Barron, J.T., Abbeel, P., Poole, B.: Zero-shot text-guided object generation with dream fields. In: CVPR, pp. 867–876 (2022)
- Jiang, C., Sud, A., Makadia, A., Huang, J., Nießner, M., Funkhouser, T., et al.: Local implicit grid representations for 3d scenes. In: Proceedings of the IEEE/CVF Conference on Computer Vision and Pattern Recognition, pp. 6001–6010 (2020)
- Kingma, D.P., Welling, M.: Auto-encoding variational bayes. arXiv preprint arXiv:1312.6114 (2013)

 Lin, C.H., Gao, J., Tang, L., Takikawa, T., Zeng, X., Huang, X., Kreis, K., Fidler, S., Liu, M.Y., Lin, T.Y.: Magic3d: High-resolution text-to-3d content creation. arXiv preprint arXiv:2211.10440 (2022)

- Luo, S., Hu, W.: Diffusion probabilistic models for 3d point cloud generation. In: CVPR, pp. 2837– 2845 (2021)
- 17. Mildenhall, B., Srinivasan, P.P., Tancik, M., Barron, J.T., Ramamoorthi, R., Ng, R.: Nerf: Representing scenes as neural radiance fields for view synthesis. Communications of the ACM **65**(1), 99–106 (2021)
- 18. Mohammad Khalid, N., Xie, T., Belilovsky, E., Popa, T.: Clip-mesh: Generating textured meshes from text using pretrained image-text models. In: SIGGRAPH, pp. 1–8 (2022)
- 19. Poole, B., Jain, A., Barron, J.T., Mildenhall, B.: Dreamfusion: Text-to-3d using 2d diffusion. arXiv preprint arXiv:2209.14988 (2022)
- 20. Qi, C.R., Su, H., Mo, K., Guibas, L.J.: Pointnet: Deep learning on point sets for 3d classification and segmentation. In: CVPR, pp. 652–660 (2017)
- 21. Rezende, D., Mohamed, S.: Variational inference with normalizing flows. In: International conference on machine learning, pp. 1530–1538. PMLR (2015)
- Sanghi, A., Chu, H., Lambourne, J.G., Wang, Y., Cheng, C.Y., Fumero, M., Malekshan, K.R.: Clipforge: Towards zero-shot text-to-shape generation. In: CVPR, pp. 18,603–18,613 (2022)
- Shen, Y., Feng, C., Yang, Y., Tian, D.: Mining point cloud local structures by kernel correlation and graph pooling. In: CVPR, pp. 4548–4557 (2018)
- 24. Shi, Z., Peng, S., Xu, Y., Liao, Y., Shen, Y.: Deep generative models on 3d representations: A survey. arXiv preprint arXiv:2210.15663 (2022)
- Tang, C., Yang, X., Wu, B., Han, Z., Chang, Y.: Part2word: Learning joint embedding of point clouds and text by matching parts to words. arXiv preprint arXiv:2107.01872 (2021)
- 26. Upadhyay, A.K., Khandelwal, K.: Metaverse: the future of immersive training. Strategic HR Review **21**(3), 83–86 (2022)
- Valsesia, D., Fracastoro, G., Magli, E.: Learning localized generative models for 3d point clouds via graph convolution. In: International conference on learning representations (2019)
- Wu, J., Zhang, C., Xue, T., Freeman, B., Tenenbaum, J.: Learning a probabilistic latent space of object shapes via 3d generative-adversarial modeling. NeurIPS 29 (2016)
- 29. Yang, G., Huang, X., Hao, Z., Liu, M.Y., Belongie, S., Hariharan, B.: Pointflow: 3d point cloud gener-

- ation with continuous normalizing flows. In: ICCV, pp. 4541–4550 (2019)
- 30. Yang, Y., Feng, C., Shen, Y., Tian, D.: Foldingnet: Point cloud auto-encoder via deep grid deformation. In: CVPR, pp. 206–215 (2018)
- 31. Zhou, L., Du, Y., Wu, J.: 3d shape generation and completion through point-voxel diffusion. In: ICCV, pp. 5826–5835 (2021)